



Stability of stainless steel unequal-leg angles with imperfect supports

Edward J. Sippel¹, Hannah B. Blum²

Abstract

Recent experimental work completed at the University of Wisconsin-Madison subjected hot-rolled and laser-fused 304 austenitic stainless steel unequal-leg angles, ranging in length from 10 inches to 148 inches, to uniform compression with fixed supports. The angles failed in flexural-torsional buckling with variable degrees of flexural and torsional deformations. This paper reports on the finite element modeling validation of the flexural-torsional buckling failures. Early work implemented a simplified approach that isolated the angle column with perfect fixed-fixed boundary conditions and incorporated measured material properties, cross-section dimensions, and geometric imperfections. This method accurately simulated the appropriate non-linear stiffness, deflection patterns, and ultimate capacities associated with the torsion-dominated buckling failures. However, the same analysis approach was not able to reproduce the reduced ductility and capacity associated with the flexure-dominated failures in this test series. Further investigation noted that the reusable loading brackets did not provide a perfect fixed support. This was a consequence of incomplete contact at the supports at the commencement of flexural buckling combined with an imperfect bearing surface. Due to the significantly high ratio of measured to nominal yield strength of the stainless steel angles, the reusable loading brackets were permanently deformed. Finite element models accounting for the incomplete contact and separation between the nonplanar bearing plates and the stainless steel angle reproduced the reduced ductility and loading capacity captured in the experimental testing. This modeling technique was used to complete a parametric study to provide data on unequal-leg angles, which highlighted the importance of defining the appropriate material model to capture accurate buckling behavior.

1. Introduction

The recent release of American Institute of Steel Construction (AISC) Specification for Structural Stainless Steel Buildings, AISC 370, (AISC, 2021) has provided additional opportunities to implement stainless steel members and take advantage of corrosion resistance, thermal properties, and aesthetics among other benefits (Houska, 2014). AISC 370 provides an updated design procedure to evaluate members in compression including compact, equal-leg single angles. Unlike carbon

¹Assistant Professor, Milwaukee School of Engineering, <sippel@msoe.edu>. Formerly, Graduate Research Assistant, University of Wisconsin-Madison

²Assistant Professor and Alain H. Peyrot Fellow, University of Wisconsin-Madison, <hannah.blum@wisc.edu>

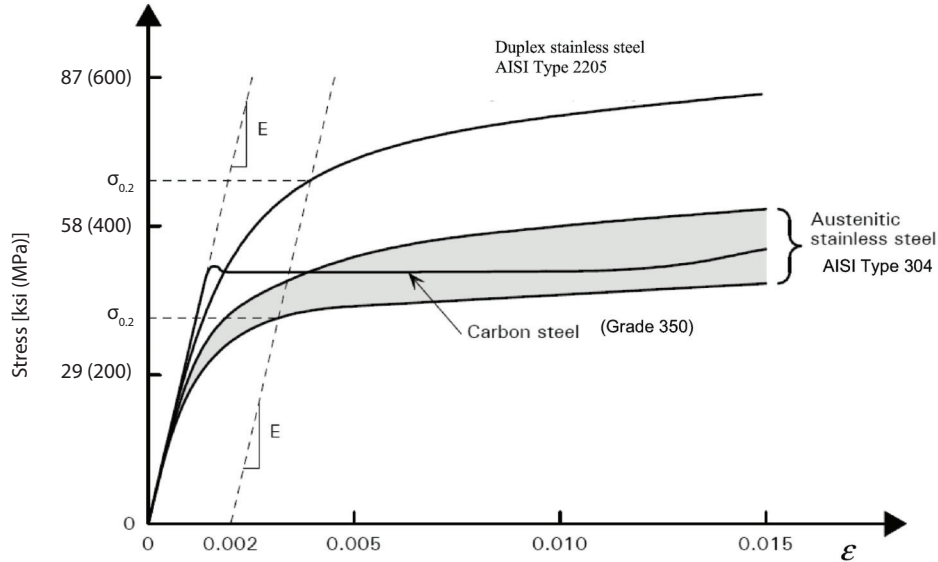


Figure 1: Typical stress-strain curves of carbon and stainless steels. (Modified from (Dundu, 2018))

steel members designed according to AISC 360 (AISC, 2016), the stainless steel provisions incorporate a three stage buckling model that separates the response into full member yield, inelastic buckling, and elastic buckling. Another modification to the design procedure is the consideration of flexural-torsional buckling with single angles. The design provisions for carbon steel single angles permit excluding the direct calculation of flexural-torsional buckling, unless the legs are highly slender, since the local buckling reduction adequately reduces the flexural buckling capacity to produce a safe design (Galambos, 1991). As a result, there is interest in expanding the available data for unequal-leg angles subjected to uniform compression such that the new provisions can be properly assessed.

1.1 Material Properties

Stainless steel exhibits a nonlinear stress-strain response, as shown in Fig. 1, unlike typical structural carbon steels. While carbon steels have a well-defined yield behavior, stainless steels have no definitive yield point. Stainless steel behavior is characterized by a departure from the linear elastic response at low stresses, which varies with the exact material grade. The yield point is alternatively defined using a specified offset strain, commonly 0.2% strain as highlighted in Fig. 1.

Various models (Dundu, 2018) have been considered to capture the nonlinear behavior of stainless steel with the most popular ones being based on the modified Ramberg-Osgood model (Hill, 1944). While this model has been shown to effectively present stresses below the yield stress, it regularly over-predicts observed stresses at higher strains as shown in Fig 2. Researchers (MacDonald and Taylor, 2000; Olsson, 2001; Mirambell and Real, 2000; Rasmussen, 2003; Gardner and Nethercot, 2004; Gardner and Ashraf, 2006; Quach, Teng, and Chung, 2008; Hradil et al., 2013) have addressed this issue in different ways; however, one of the more common solutions is the application of a two-stage, modified Ramberg-Osgood stress-strain relationship as shown in Eq. 1:

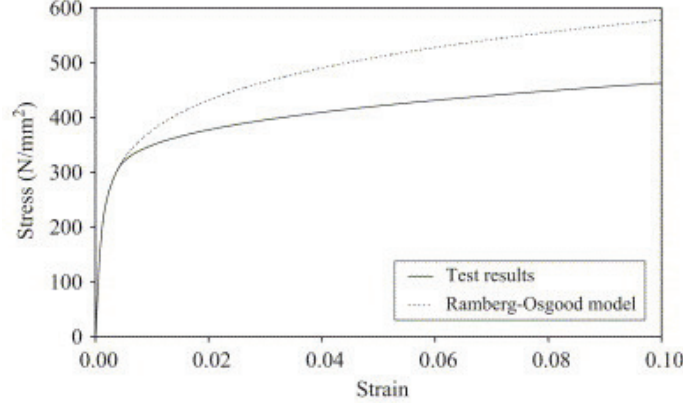


Figure 2: Comparison of modified Ramberg-Osgood model and experimental stress-strain curves (Ashraf, Gardner, and Nethercot, 2006)

$$\epsilon = \begin{cases} \frac{\sigma}{E_0} + 0.002 \left(\frac{\sigma}{\sigma_{0.2}} \right)^n & \text{if } \sigma \leq \sigma_{0.2} \\ \frac{\sigma - \sigma_{0.2}}{E_{0.2}} + \epsilon_{\max} \left(\frac{\sigma - \sigma_{0.2}}{\sigma_{\max} - \sigma_{0.2}} \right)^{n_{0.2, \max}} + \frac{\sigma_{0.2}}{E_{0.2}} + 0.002 & \text{otherwise} \end{cases} \quad (1)$$

where ϵ is the current strain, σ is the current stress, $\sigma_{0.2}$ is the 0.2% offset yield stress, E_0 is the initial modulus of elasticity, n is the strain hardening exponent, $E_{0.2} = E_0 / (1 + 0.002nE_0/\sigma_{0.2})$ is the tangent modulus of elasticity at $\sigma_{0.2}$, σ_{\max} is the maximum reference stress, ϵ_{\max} is the maximum reference strain, and $n_{0.2, \max}$ is the Ramberg-Osgood strain-hardening coefficient for the second stage.

1.2 Compression Testing

The buckling behavior of concentrically loaded angles has been studied for a number of years. The majority of research has focused on carbon steel equal-leg angles with some consideration of stainless steel or unequal-leg geometries. However, work considering stainless steel unequal-leg angles was not located.

1.2.1 Stainless Steel Equal-Leg Angles

In recent years, research on stainless steel equal-leg angles subjected to uniform compression has become an active topic. Before this, Kuwamura (2003) and Sun et al. (2019) provided some of the limited relevant results. Kuwamura (2003) was primarily concerned with the local buckling behavior of thin-walled stainless steel sections. As part of that study, twelve cold-formed austenitic equal-leg angle stub-columns were tested to failure with nominally fixed-fixed end conditions. Flexural-torsional buckling was observed at failure of the columns with compact cross sections having ultimate loads greater than the yield stress. As the slenderness of individual legs increased, the buckling load decreased and was found to be less than the yield stress for slender legs. As part of a study on laterally constrained bending behavior of hot-rolled stainless steel equal-leg angles, Sun et al. (2019) similarly completed a series of stub-column tests. All ten tests were also found to exhibit flexural-torsional buckling with most exceeding the nominal yield stress.

Reynolds (2013) investigated the behavior of laser-welded duplex equal-leg angles. Thirty-three

specimens were subjected to concentric compression with the ends pinned for weak-axis bending, fixed for strong-axis bending, and fixed for warping. Weak-axis flexural buckling was observed in 28 of the specimens, while the remaining five were found to exhibit flexural-torsional buckling. Reynolds found that the evaluation of flexural-torsional buckling design provisions resulted in overly conservative results, while the accuracy of flexural buckling provisions varied among different specifications. A parametric study using shell elements indicated the flexural-torsional buckling became increasingly critical as the cross-section slenderness increased.

Liang et al. (2019) subjected 16 fixed-ended hot-rolled austenitic stainless steel equal-leg angles to concentric compression. All members depicted flexural-torsional buckling, but longer members also incorporated an interaction with flexural buckling. The experimental results and a complementary finite element parametric study were compared to existing design provisions and indicated that flexural-torsional buckling was conservatively predicted. Comparisons to proposed direct strength method provisions for flexural-torsional buckling, which were based on carbon steel behavior, resulted in improved accuracy of the expected capacity. However, approximately half of the estimated capacities were unconservative due to not accounting for the softer material response of stainless steel compared to carbon steel. A comparable study completed by Siqueira et al. (2020) with 18 fixed-end hot-rolled austenitic stainless steel equal-leg angles obtained similar conclusions. Additional numerical work with slender equal-leg angles noted that observed local buckling did not correspond with the behavior indicated by the Eurocode 3 provisions (Sarquis et al., 2020).

An extended series of compression tests were completed at the University of Belgrade including hot-rolled (Filipović, Dobrić, Baddoo, et al., 2021), laser welded (Filipović, Dobrić, Buđevac, et al., 2021), and cold-formed (Dobrić et al., 2020) stainless steel equal-leg angles. All columns were fixed for strong-axis bending and torsion while pinned for weak-axis bending. The measured yield stress was consistently found to exceed the specified nominal value with the largest variation of 55% noted for the hot-rolled sections. The shorter stub column tests were found to fail in flexural-torsional buckling. The slender cold-formed section exhibited failure below the yield stress, while the laser welded and hot-rolled specimens exceeded the yield stress. Flexural-torsional buckling was observed throughout the shorter specimens with a gradual transition to flexural buckling behavior at long lengths. The test results indicated that existing design procedures resulted in safe, but inaccurate strength predictions. These design calculations only considered flexural buckling, which aligned with the recommendation of the first edition of the AISC Design Guide 27 (Baddoo, 2013) to not consider flexural-torsional buckling.

Another test series of 24 hot-rolled stainless steel equal-leg angles including short and long member lengths studied by Zhang, Liang, and Zhao (2020; 2021) observed similar global buckling behaviors and inaccurate strength predictions by existing design procedures.

Behzadi-Sofiani, Gardner, and Wadee (2021) completed an experimental and numerical study on fixed-end stainless steel equal-leg angle columns. The flexural buckling controlled capacities were reasonably estimated using existing design provisions, but flexural-torsional buckling could be widely underestimated. They noted that the flexural-torsional buckling behavior of columns can be effectively double counted in column design based on current practices considering combined global and local buckling.

1.2.2 Unequal-Leg Angles

Despite the growing database for equal-leg angles, only minimal existing research on unequal-leg angles subjected to uniform compression, including none for stainless steel members, was located. Early work by Liu and Chantel (2011) considered 26 carbon steel unequal-leg angles subjected to compression with varying amounts of eccentricity. All five concentrically loaded angles failed primarily in flexural buckling at less than 40% of the yield stress. Dinis et al. (2015) evaluated four carbon steel unequal-leg angles to investigate the elastic flexural-torsional response in asymmetric sections. Experimental results and subsequent modeling were found to be in agreement with the standard theoretical elastic buckling capacity used in the AISC Specifications. Ojalvo (2011) summarized the results of three fixed end aluminum unequal-leg angles tests (Liao, 1982; Wu, 1982). The inelastic response of the fixed ended columns captured additional post-critical strength excluded in standard elastic buckling assumptions. Recently, Zhang, Wang, et al. (2020) and Zhang, Bu, et al. (2021) tested a combined 22 pinned end aluminum unequal-leg angle columns. Experimental results consistently exhibited flexural-torsional buckling. The response was dominated by torsional behavior at short lengths with a gradual transition to significant flexural behavior at long lengths.

1.3 Design Provisions

In the late 1800's, Engesser demonstrated how inelastic buckling capacity could be determined by considering the tangential stiffness of a perfectly straight column, which was in agreement with experimental results (Timoshenko and Gere, 1961). This approach still serves as the basis behind current methods including the AISC Structural Stainless Steel Specification (AISC, 2021). These provisions capture this phenomenon by converting the elastic buckling stress, F_e , into the critical buckling stress, F_{cr} . Since stainless steel is a more expensive material, the desire for efficient material usage has resulted in buckling being defined by a three-stage response. Similar to carbon steel, low compressive stresses correspond to an elastic buckling behavior with minor reduction for imperfections and residual stresses. As the stress increases, the response transitions to include inelastic buckling behavior. Unlike carbon steel, designs with stainless steel allow for full yield in compression at short lengths. Based on existing research, Meza, Baddoo, and Gardner (2021) developed the current flexural design provisions for compression members, given by Eq. 2:

$$F_{cr} = \begin{cases} F_y & \text{if } \frac{F_y}{F_e} \leq \left(\frac{\beta_0}{\pi}\right)^2 \\ 1.2 \left[\beta_1 \left(\frac{F_y}{F_e}\right)^\alpha \right] F_y & \text{if } \left(\frac{\beta_0}{\pi}\right)^2 < \frac{F_y}{F_e} \leq 3.20 \\ \beta_2 F_e & \text{if } \frac{F_y}{F_e} > 3.20 \end{cases} \quad (2)$$

where α , β_0 , β_1 , β_2 are flexural buckling coefficients that vary based on the member type as shown in Table 1. Multiple column curves have been adopted to capture the increased strength associated with different cross sections buckling.

Following AISC 370, single angle compression member design is limited to equal-leg, compact cross sections. Despite the current buckling coefficients being based on flexural buckling, the design procedures require the determination of the minimum controlling elastic global buckling behavior including flexural-torsional buckling, which is then adjusted using Eq. 2 with Curve A

Table 1: Flexural buckling coefficients for stainless steel

Member Type	Curve	α	β_0	β_1	β_2
I-shaped sections buckling about the minor axis and other sections not specified in this table	A	0.56	0.759	0.409	0.690
I-shaped sections buckling about the major axis, welded box sections, and round HSS	B	0.58	0.891	0.455	0.820
Rectangular HSS	C	0.69	1.195	0.501	0.820

Table 2: Experimental mechanical properties

Curve #	Specimen	E_0 (ksi)	σ_y (ksi)	$\sigma_{1.0}$ (ksi)	n	$n_{0.2,1.0}$
1	SC10-1	28745	52.6	64.7	5.35	2.57
2	SC10-2	27779	38.9	50.9	4.23	2.20
3	SC10-3	28353	43.4	46.2	10.45	1.51
4	SC18-1	25755	54.9	63.5	8.78	2.12
5	SC18-2	27799	54.5	62.3	9.13	2.55
6	SC18-3	27757	46.1	53.7	8.83	2.29
Average		27698	48.4	56.9	7.80	2.21

coefficients from Table 1. The singly symmetric geometry of equal-leg angles normally exhibit flexural buckling about the weak-axis at longer lengths with a transition to flexural-torsional buckling at short lengths. This transition is typically associated with a significant drop in buckling capacity compared to the flexural buckling response. While not covered by the current AISC 370, an asymmetric unequal-leg angles would behave similarly, in that flexural behavior dominates at long lengths which then transitions to torsional behavior at short lengths. However, the controlling response is always a flexural-torsional buckling, which means there is consistently an additional reduction applied to the buckling capacity.

An interesting phenomenon in single angles is the equivalency of flexural-torsional buckling and local buckling, both in terms of the deformed shape and buckling capacity (Rasmussen, 2005; Behzadi-Sofiani, Gardner, and Wadee, 2021). As a result, existing design provisions run the risk of double counting the same effect when evaluating flexural-torsional buckling and local buckling in single angles. This issue is addressed in AISC 360 for carbon steel members (AISC, 2016) by not requiring flexural-torsional buckling to be considered in compression member design for single angles. Galambos (1991) demonstrated that carbon steel single angles could safely be designed using the flexural buckling capacity reduced for local buckling concerns. This provision was carried forward to the original AISC Stainless Steel Design Guide (Baddoo, 2013) as it was modeled after AISC 360 with additional reductions for the nonlinear behavior of stainless steel. However, that exception was not incorporated into the current AISC 370 or updated Design Guide.

2. Experimental Data

This computational study utilized the hot-rolled stainless steel unequal-leg angle compression testing program completed at the University of Wisconsin - Madison (Laracuate, Sippel, and Blum, 2022; Laracuate, 2022). As part of the preliminary investigation, the stress-strain behavior of the 304/304L stainless steel angles was measured via six tensile coupon tests taken around the cross section of two different specimen. Table 2 summarizes the best fit of the experimental results using a two-stage modified Ramberg-Osgood model using a 1% maximum strain as reference point in line with Arrayago, Real, and Gardner (2015).

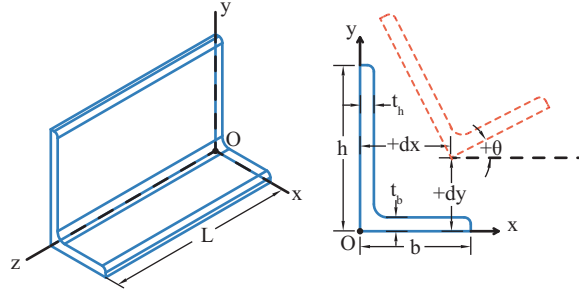


Figure 3: Unequal-leg angle conventions for dimensions, axes, and displacements

Table 3: Measured geometric properties of test specimens

Specimen	L (in)	b (in)	h (in)	t_b (in)	t_h (in)	Area (in ²)
S10-A1-1	10	2.049	2.979	0.257	0.266	1.251
S10-A2-1	10	2.055	2.977	0.258	0.243	1.191
S10-A2-2	10	2.052	2.966	0.258	0.244	1.192
S20-A1-1	20	2.030	2.981	0.253	0.253	1.203
S20-A2-1	20	2.063	2.958	0.258	0.241	1.182
S20-A2-2	20	2.063	2.965	0.259	0.243	1.190
S36-A1-1	36	2.019	2.985	0.251	0.253	1.198
S36-A1-2	36	2.014	2.991	0.251	0.253	1.198
S36-A2-1	36	2.076	2.964	0.259	0.241	1.190
S72-A5-1	72	2.005	2.987	0.250	0.250	1.185
S72-A5-2	72	2.010	2.985	0.251	0.249	1.184
S72-A6-1	72	2.034	2.980	0.253	0.256	1.214
S100-A3-1	100	2.057	2.957	0.258	0.252	1.210
S100-A4-1	100	2.067	2.933	0.258	0.252	1.208
S100-A4-2	100	2.063	2.939	0.258	0.253	1.209
S148-A1-1	147-15/16	2.006	2.999	0.249	0.254	1.199
S148-A2-1	147-15/16	2.033	2.972	0.256	0.244	1.182
S148-A3-1	147-15/16	2.020	2.989	0.255	0.254	1.210

The main experimental series evaluated 18 hot-rolled stainless steel L3×2×1/4, which included three specimens at six different lengths. The specimen are labeled S‘XX’-A‘Y’-‘N’ based on the nominal length, ‘XX’, the stock angle id, ‘Y’, and ‘N’ identifies multiplies from the same stock. Prior to testing, the dimensions of the angles were obtained by hand. Table 3 summarizes the measured dimensions, where L is the length of the specimen, b and h are the width and height of the section, respectively, and t_b and t_h are the corresponding leg thicknesses as depicted in Fig. 3. The imperfections along the length of the specimen were measured using non-contact laser methods (Laracuente, Sippel, and Blum, 2022; Sippel, 2022) with the maximum imperfections summarized in Table 4. As illustrated in Fig. 3, dx and dy are the lateral imperfection in the x- and y- direction at the heel of the angle, and $d\theta$ is the rotation of the cross-section.

2.1 Compression Tests

The full-scale compression tests were completed using a Southwark Emery Testing Machine with a 1 million pound capacity. As illustrated in Fig. 4, the tests were completed with nominal fixed-fixed boundary conditions using reusable 50 ksi base plates. Before starting the test series, the base plates and end of each angle were milled flat to provide full end bearing. Three 3/4" thick, A36 clamping brackets were then used to lateral position angle. All test specimens were observed

Table 4: Maximum measured imperfections

Specimen	Measured			Normalized		
	dx (in)	dy (in)	θ (deg)	dx/(L/1000)	dy/(L/1000)	$\theta/\tan^{-1}(L/1000h)$
S10-A1-1	-0.014	-0.007	-0.20	-1.434	-0.705	-1.05
S10-A2-1	0.003	0.002	0.04	0.347	0.197	0.21
S10-A2-2	0.003	0.002	N/A ¹	0.300	0.150	N/A ¹
S20-A1-1	-0.016	-0.013	-0.22	-0.787	-0.639	-0.56
S20-A2-1	-0.006	-0.003	0.04	-0.288	-0.160	0.09
S20-A2-2	0.005	-0.009	0.05	0.236	-0.442	0.13
S36-A1-1	0.018	-0.018	-0.12	0.494	-0.499	-0.17
S36-A1-2	-0.011	-0.036	-0.18	-0.299	-1.000	-0.26
S36-A2-1	-0.048	-0.022	-0.21	-1.339	-0.603	-0.31
S72-A5-1	0.063	-0.064	0.26	0.873	-0.893	0.19
S72-A5-2	-0.142	-0.134	0.15	-1.978	-1.857	0.11
S72-A6-1	0.035	-0.037	0.10	0.483	-0.520	0.07
S100-A3-1	0.218	0.070	-0.30	2.183	0.695	-0.16
S100-A4-1	0.086	-0.073	-0.37	0.858	-0.732	-0.19
S100-A4-2	-0.037	-0.126	0.35	-0.369	-1.259	0.18
S148-A1-1	-0.070	-0.141	-0.20	-0.472	-0.955	-0.07
S148-A2-1	0.470	0.206	-0.33	3.178	1.389	-0.12
S148-A3-1	0.287	-0.070	-0.20	1.943	-0.474	-0.07

¹ Hand measurements provided. Results from scanned data not available due to poor scan quality.

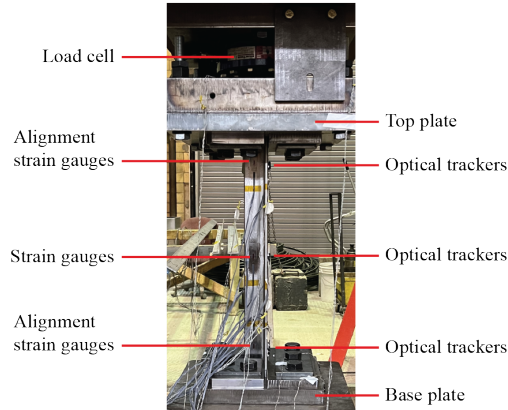


Figure 4: Typical compression testing set-up

to exhibit flexural-torsional buckling at the failure loads summarized in Table 5. The buckling response was dominated by torsional deformations for short specimens, which transitioned to flexural bending for longer ones.

3. Computational Study

3.1 Modeling Methodology

Using the experimental discussed above, the modeling approach for an unequal-leg angle was validated before completing a parametric study. The reference $L3 \times 2 \times 1/4$ specimens were evaluated using finite element analysis via Abaqus (Dassault Systems, 2015b). The unequal-leg cross sections were modeled as S4R shell elements, which has a four node linear formulation with reduced integration, hour-glass control, and a general formulation that includes both thick and thin shell behavior (Dassault Systems, 2015a). This approach aligned with previous works (Reynolds, 2013;

Table 5: Experimental failure loads compared to design loads using nominal and measured material properties

Specimen	Load (kip)	Specimen	Load (kip)	Specimen	Load (kip)
S10-A1-1	62.1	S36-A1-1	57.1	S100-A3-1	19.2
S10-A2-1	69.5	S36-A1-2	52.7	S100-A4-1	18.4
S10-A2-2	68.8	S36-A2-1	53.3	S100-A4-2	18.0
S20-A1-1	61.3	S72-A5-1	30.8	S148-A1-1	7.8
S20-A2-1	66.8	S72-A5-2	24.8	S148-A2-1	5.6
S20-A2-2	65.4	S72-A6-1	34.4	S148-A3-1	6.7

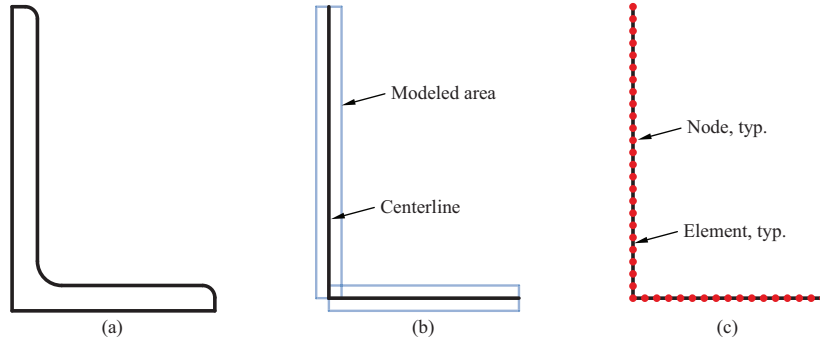


Figure 5: Typical model of unequal-leg cross section. (a) Actual cross section. (b) Modeled cross section. (c) Meshed cross section

Liang et al., 2019; Sirqueira et al., 2020; Behzadi-Sofiani, Gardner, and Wadee, 2021; Zhang, Tan, and Zhao, 2019; Zhang, Liang, and Zhao, 2020; Zhang, Liang, and Zhao, 2021; Dinis et al., 2015; de Menezes et al., 2019) that have shown shell elements can be used to accurately model single angles in compression.

The unequal-leg geometry was modeled using the centerline model shown in Fig. 5(b) using centered elements, which has shown to provide comparable computational results compared to solid element models (Reynolds, 2013; Dinis et al., 2015). Based on a refinement study, the member was modeled using a square mesh with 16 elements across the short flange with equivalent sized elements on the long flange as indicated in Fig. 5(c). The end boundary condition for the unequal-leg angle models was applied using a single reference node at the angle centroid that was connected to all nodes across the end of the angle through a rigid tie constraint. As a result, the angle was always full constrained against warping, and the flexural boundary condition could be readily defined as fixed or pinned in the geometric orientations. For the validation analysis, the end of the member was fixed for bending about both axes.

The material model for this study was selected from the experimental results listed in Table 2. Evaluating the axial response of the 10-inch columns, which correspond to typical stub column test geometry, stress-strain curve #5 from Table 2 was selected as it best captured the ultimate capacity, initial modulus of elasticity, and intermediate stiffness as depicted in Fig. 6. This behavior was implemented in the finite element analysis using an elastic-plastic model that ignored the initial $(0.5\text{ksi})/E_0$ plastic strain to minimize the concerns of underestimating capacity noted by Schafer, Li, and Moen (2010).

Four variations of the measured imperfections were evaluated, as summarized in Table 6, to investigate the effect of the imperfection shape. Rotation and translations were treated as distributions

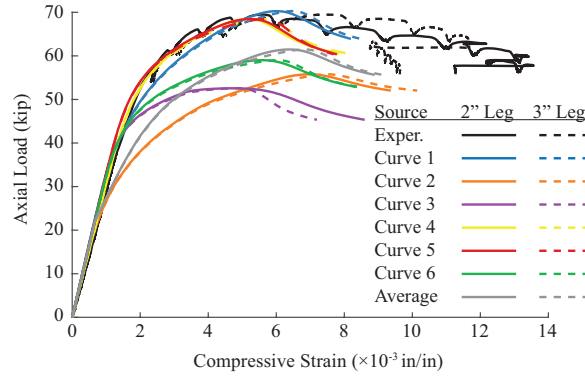


Figure 6: Applied axial load-strain response of S10-A2-1 column

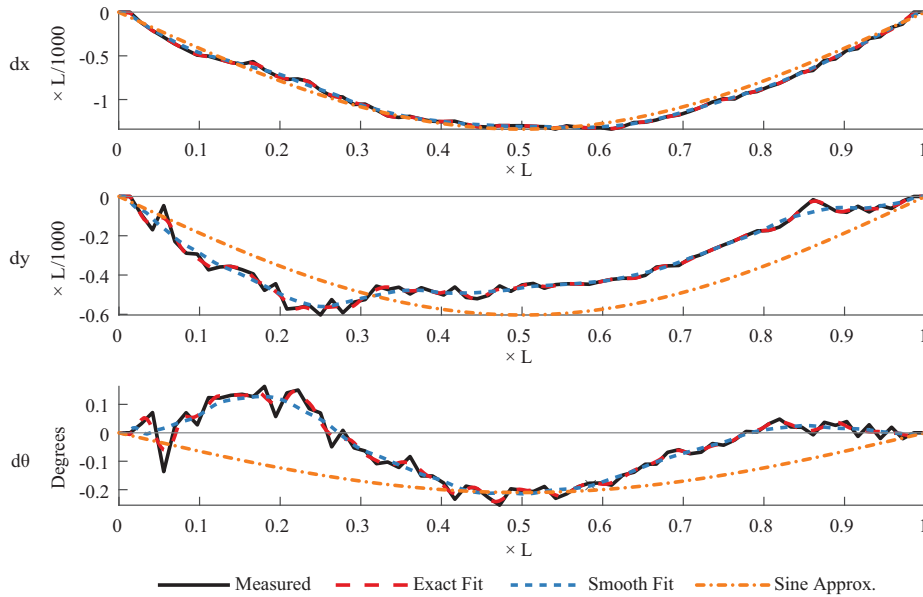


Figure 7: Initial imperfections as adjusted for finite element modeling for S36-A2-1

that could be separately applied to determine the importance of including the rotation imperfection that is occasionally excluded in parametric studies. Additionally, the imperfection profile was applied as a “Smooth” or “Sine” profile as shown in Fig. 7. The “Sine” profile applied a traditional half-sine curve profile based on the maximum value noted in Table 4. The “Smooth” profile accounted for the variable imperfection along the length of the specimen. The profile was interpolated from the measured profile to fit the underlying finite element mesh. This process included a smoothing filter to eliminate localized kinks that created unrealistic stress concentrations.

3.2 Validation Results

The results of the validation study are provided in Table 7. The computational models matched well with the experimental results for all specimen 72 inches and shorter. The simulation was able to replicate the torsional buckling dominant response in short columns as shown in Fig. 8. The inclusion of additional flexural movement as the column length increased was also captured as depicted in Fig. 9. However, as the buckling transitioned to a primarily flexural buckling response at long lengths, see Fig. 10, significant variations between the modeled and actual response were

Table 6: Imperfection Distributions considered in Validation Study

Label	Translations		Rotations	
	Smooth	Sine	Smooth	Sine
IV-1	x			
IV-2	x		x	
IV-3	x			x
IV-4		x		x

Table 7: Ultimate failure loads for validation modeling with variable imperfections

Specimen	Test (kip)	Ultimate load (kip) with			
		IV-1	IV-2	IV-3	IV-4
S10-A1-1	62.1	70.3	69.5	69.5	69.6
S10-A2-1	69.5	68.9	68.4	68.4	68.4
S10-A2-2	68.8	69.1	69.1	69.1	69.1
S20-A1-1	61.3	62.0	61.4	61.5	61.6
S20-A2-1	66.8	63.4	63.5	63.6	63.3
S20-A2-2	65.4	63.5	63.5	63.3	63.0
S36-A1-1	57.1	53.0	53.1	53.2	53.7
S36-A1-2	52.7	54.4	54.0	53.9	52.9
S36-A2-1	53.3	51.7	51.3	51.4	51.3
S72-A5-1	30.8	33.2	33.0	32.9	33.4
S72-A5-2	24.8	28.3	28.3	28.4	28.4
S72-A6-1	34.4	35.1	35.1	35.0	36.7
S100-A3-1	19.2	19.1	19.1	19.1	19.2
S100-A4-1	18.4	22.9	22.9	23.0	22.9
S100-A4-2	18.0	22.4	22.6	22.7	22.2
S148-A1-1	7.8	10.4	10.4	10.4	10.2
S148-A2-1	5.6	9.1	9.1	9.1	9.0
S148-A3-1	6.7	9.9	9.9	9.9	9.9
Full Series	Mean	1.12	1.12	1.12	1.12
	CoV	0.17	0.17	0.17	0.17
0"-72" Series	Mean	1.02	1.02	1.02	1.02
	CoV	0.06	0.06	0.07	0.07

noted. The desired primary behavior was captured, but at higher magnitudes and more gradually in the computational result.

While investigating the different response, the larger flexural deformation of the buckled column combined with the fixed boundary condition was observed to cause tension to develop at the end of the specimens in the finite element analysis. While reasonable, this behavior was unrealistic as bearing would be lost if tensile flexural stresses exceeded the axial compression. Exploratory work to directly account for contact at the base plate confirmed that uplift did occur at buckling for the longer specimens. Most investigations noted the angle lifted at the heel, which increased the bearing stress at the tip causing more localized yielding of the angle. A slightly reduced ultimate capacity and less post-buckling ductility were also noted, but not enough to match the experimental results. A closer inspection of the base plates after the compression tests noted that there was permanent deformation as shown in Fig. 11. While it was not anticipated that the base plates would plastically deform under ultimate loads based on the nominal stainless steel yield strength, the actual experimental yield strength was measured as 60% greater than nominal (Laracuate, Sippel, and Blum, 2022), which caused small impressions on the base plates under

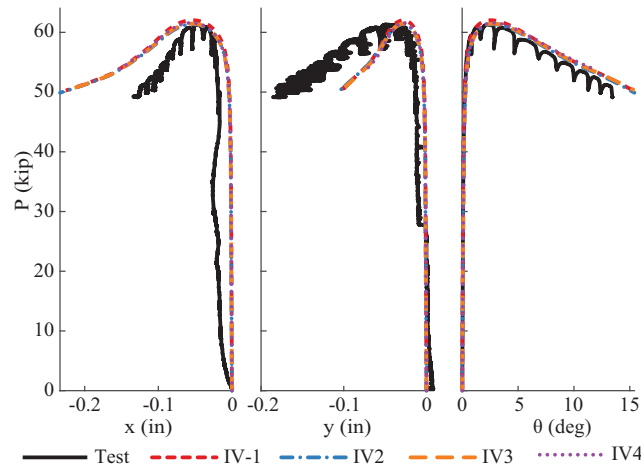


Figure 8: Torsion dominated buckling displacement of S20-A1-1

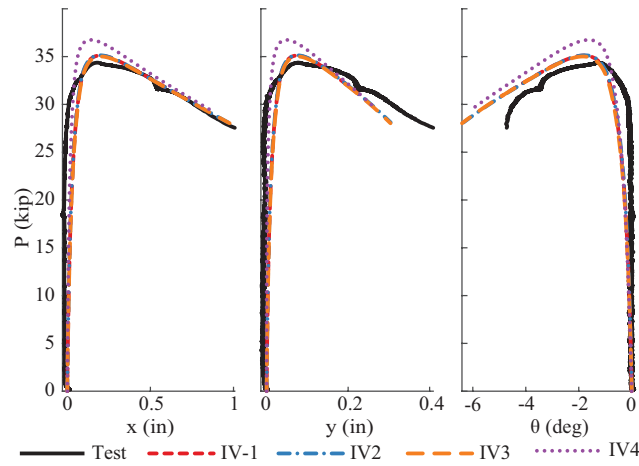


Figure 9: Intermediate flexural-torsional buckling displacement of S72-A6-1

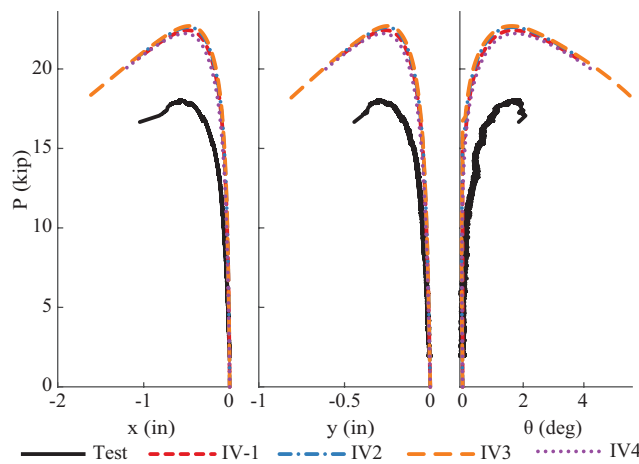


Figure 10: Flexure dominated buckling displacement of S100-A4-2

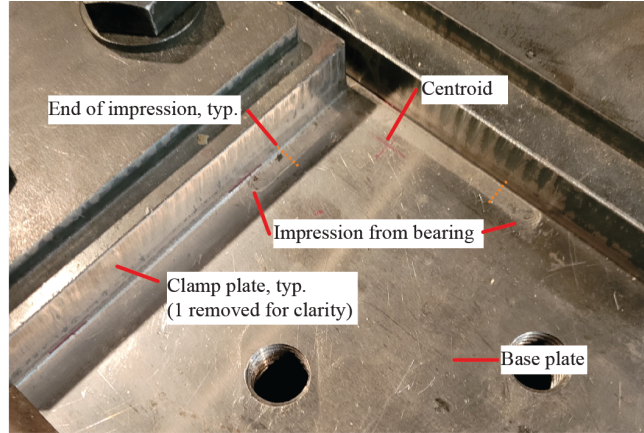


Figure 11: Base plate after final compression test series

Table 8: Angles in Parametric Study

L6"×5"×1/2"	L6"×4"×1/2"	L6"×3"×1/2"	L5"×3"×1/2"	L4"×3"×1/2"	L4"×3"×3/8"
L3"×2"×3/8"	L3"×2"×1/4"	L3"×1-1/2"×1/4"	L2"×1-1/2"×1/4"	L2"×1"×1/4"	L1-1/2"×1-1/4"×1/8"

the tips of each angle leg. While the high stresses of the short columns affected the entire bearing area, the primary concern was the tips of each leg where the final 0.63 inch of each leg was clearly deformed, varying approximately linearly to a max impression of 0.02 inch at the tip. Finite element modeling incorporating contact, the imperfect bearing surface, and deformation of the base plate resulted in only minor changes for shorter columns; however, the majority of 100-inch and 148-inch models captured a significantly reduced capacity, less overall deflection, and partial bearing. Acknowledging the limitation of the modeling approach, the validation study indicated that the modeling approach was capable of depicting the behavior of stainless steel unequal-leg angles with perfect boundary conditions, and thus acceptable to implement in a parametric study.

4. Parametric Study

A parametric study was completed to expand the available data for unequal-leg single angles. In total twelve compact representative unequal-leg angles, listed in Table 8, were selected to cover typical h/t , b/t , and h/b ratios of the 50 compact cross sections that are currently available for purchase or listed in the AISC carbon steel design manual (AISC, 2017).

Each cross section was evaluated with nominal dimensions, nominal imperfections, and an effective slenderness ratio, L_e/r_z , ranging from 5 to 200. The nominal imperfections were half-sine wave imperfections with a magnitude of $L/1000$ in the negative x- and y-directions and a rotation of $-\tan^{-1} L/(1000h)$, but limited to 1° . All cross sections were modeled for both a fixed-fixed, $0.5L = L_e$, and pinned-pinned, $1.0L = L_e$, boundary condition. The angles were then modeled with either the measured material properties, matching the validation study, or nominal material properties for 304 or 304L based on the AISC list nominal values (AISC, 2021). In the total 2,880 models, flexural-torsional buckling was consistently observed. Similar to the experimental results in Section 2., flexural deformation were dominant at high slenderness ratios that transitioned to torsional deformation as the slenderness ratio decreased. Due to the selected imperfection, a few geometries noted a deviation from the typical flexural buckling response as shown in Fig. 12;

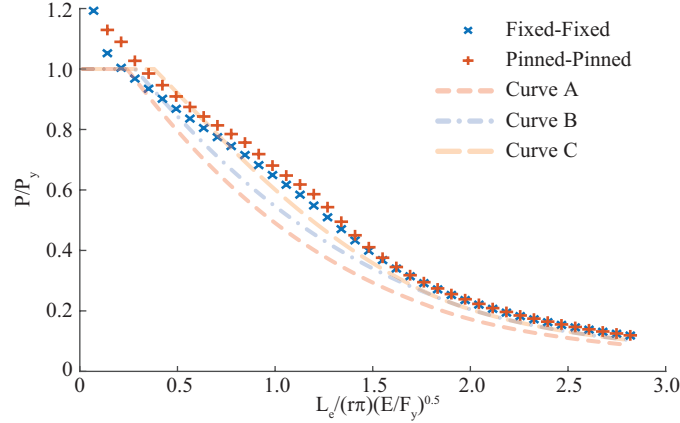


Figure 12: Buckling behavior of L6"×4"×1/2" with measured material properties versus AISC 370 buckling curves

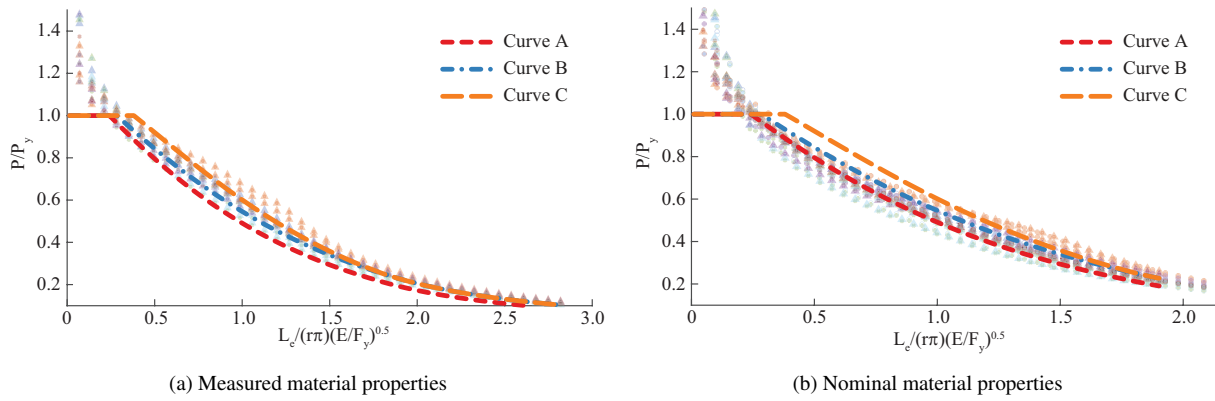


Figure 13: Buckling behavior with different material properties

however, this consistently corresponded with an increase in capacity relative to the design flexural buckling curve, not the decrease typically associated with including flexural-torsional buckling.

5. Discussion

The parametric study resulted in distinct variations depending on the material properties considered. Using the AISC 370 flexural buckling relationships as a reference, Table 1, the measured material property results were found to be normally greater than Curve A, the applicable parameters to single angles, Fig. 13a, while a number of nominal material property results were determined to be lower than Curve A, Fig. 13b. By comparing the effective stiffness included in each model in Fig. 14, there is a distinct variation between the nominal assumed behavior and the measured behavior used in this study. The increased strain-hardening coefficient measured in this study, which agrees with previous research on hot rolled sections (Behzadi-Sofiani, Gardner, and Wadee, 2021; Liang et al., 2019; de Menezes et al., 2019; Sun et al., 2019), caused a stiffer material response.

This variation within the parametric study due to the measured and material properties is further highlighted when comparing the simulated column capacity, P_{SIM} , to the compression capacity from AISC 370 design provisions with the corresponding yield stress and considering flexural buckling, P_{FB} , or flexural-torsional buckling, P_{FTB} . For the nominal material properties, flexural buckling capacity alone was observed to be a poor predictor of capacity for multiple sections at

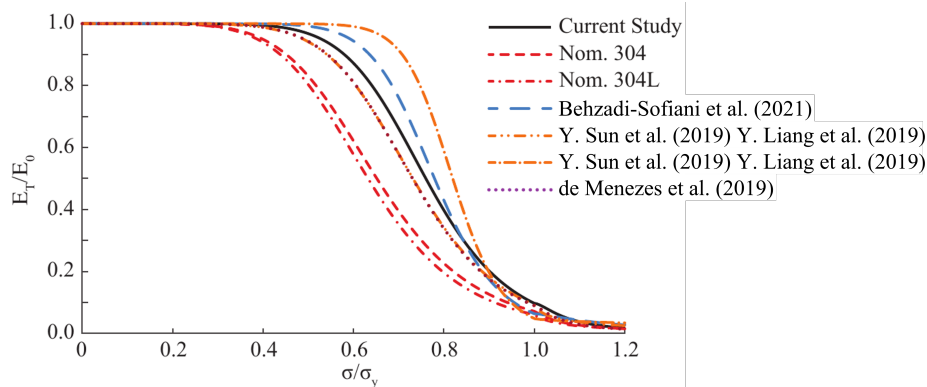
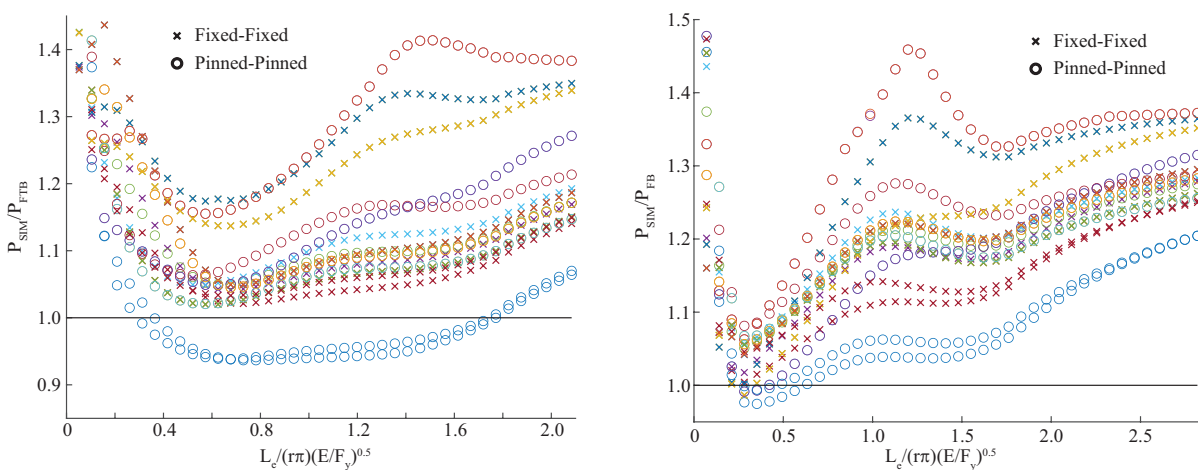


Figure 14: Effective modulus of elasticity within material models



(a) Nominal 304 with current design provision

(b) Measured 304 considering only flexural buckling

Figure 15: Nominal 304 modeled capacity versus design flexural-torsional buckling

shorter lengths, and it was necessary to include flexural-torsional buckling effects to conservatively estimate the majority of cross sections as shown in Fig. 15a. This contrasts with the measured material property results that indicate that flexural buckling alone was an adequate predictor of strength, Fig. 15b. Note that this flexural buckling prediction could be improved further if local buckling was considered as the increased yield stress would reclassify some cross sections as slender.

The varied results of the parametric study highlighted the importance of defining the appropriate material response. With carbon steel sections, the majority of steel grades used for structural design exhibit a consistent material behavior that is readily simplified to an approximate elastic-plastic response. Despite a simple, consistent material model, multiple compression design curves have been developed that vary with the cross-section shape being analyzed (Ziemian, 2010). This issue is complicated for stainless steel members as the variability of the nonlinear constitutive relationship adds an additional dimension. The nominal stress-strain relationship has experimental backing that it is appropriate for the baseline behavior of 304/304L stainless steel in a very broad range of applications. However, additional research, including the testing related to this study, has regularly noted significant increases in strength and stiffness when investigating structural stainless

steel sections as highlighted in Fig. 14. As a result, the three design curves in AISC 370 are attempting to balance the impact of different geometries, including the variable cross sections and typical imperfections as had been done with carbon steel, as well a realistic, average response of typical stainless steel members. Therefore, the trends observed in all the completed simulations are useful information, but evaluations of the design provisions first requires assessing if the nominal AISC material model is appropriate for the behavior of structural members.

Due to this observation, the completed study cannot directly assess the appropriateness of the buckling coefficients given in Curve A for compression design from AISC 370 for unequal-leg angles in general. Curve A parameters were determined to be conservative for this batch of stainless steel angles. However, stainless steel members that only meet the minimum grade requirements could be under designed with these buckling coefficients. Despite that limitation, this parametric study agrees with previous research on equal-leg single angles that directly accounting for flexural-torsional buckling underestimates the capacity of single angles. The straight-forward simplification considered in design to use the same elastic-to-critical buckling stress calculation for both flexural and flexural-torsional buckling becomes less appropriate as a greater component of the total capacity relies on the torsional shear behavior. Therefore, implementation of a provision similar to what currently applies to carbon steel should be considered. Allowing single angles to be designed by only evaluating flexural buckling with local buckling reductions, thereby relying on the indirect evaluation of flexural-torsional buckling, would allow for a more efficient use of material. While further work is needed to assess the appropriateness of local-buckling provisions for all slender cross sections, the limited results in this study noted similarity to the carbon steel angle observations that the flexural buckling capacity was adequately reduced when flexural-torsional buckling is applicable.

6. Conclusions

This study investigated the flexural-torsional buckling behavior of stainless steel unequal-leg single angles. A modeling procedure was developed and validated by comparison to experimental results from 18 fixed-fixed 304/304L L3"x2"x1/4" columns with lengths ranging from 10 inches to 148 inches. The subsequent parametric study considered 12 cross sections, nonslender for nominal material properties, with a L_e/r_z ratio ranging from 5 to 200 to incorporate elastic and inelastic failures. Each cross section was evaluated for a fixed-fixed and pinned-pinned flexural end restraint and one of three material models based on either nominal 304 parameters, nominal 304L parameters, or the measured material properties determined through the validation study. The simulations captured flexural-torsional buckling of all cross sections with both flexural and torsional dominated failures. It was determined that the existing buckling coefficients for generic cross-sections produced conservative results when considering measured material properties. While flexural-torsional buckling was consistently observed, evaluation of existing flexural-torsional buckling design provisions resulted in excessive conservatism in design for most applications. It was determined that evaluating flexural buckling with local buckling reductions, similar to the design provisions for carbon steel single angles, addressed most flexural-torsional buckling concerns for the stainless steel single angles in this study. Additional work should focus on slender cross sections to validate the consistency of this result and to determine if a limiting slenderness of the cross section is applicable.

References

- AISC (2016). *Specification for Structural Steel Buildings ANSI/AISC 360-16*. Chicago, IL: American Institute of Steel Construction, p. 676.
- AISC (2017). *Steel Construction Manual*. 15th ed. Chicago, IL: American Institute of Steel Construction.
- AISC (2021). *Specification for Structural Stainless Steel Buildings ANSI/AISC 370-21*. Chicago, IL: American Institute of Steel Construction, p. 376.
- Arrayago, I., E. Real, and L. Gardner (2015). “Description of stress–strain curves for stainless steel alloys”. In: *Materials & Design* 87, pp. 540–552. DOI: <https://doi.org/10.1016/j.matdes.2015.08.001>.
- Ashraf, Mahmud, Leroy Gardner, and D. A. Nethercot (2006). “Compression strength of stainless steel cross-sections”. In: *Journal of Constructional Steel Research* 62.1-2, pp. 105–115. DOI: [10.1016/j.jcsr.2005.04.010](https://doi.org/10.1016/j.jcsr.2005.04.010).
- Baddoo, Nancy R. (2013). *Structural Stainless Steel*. Design Guide 27. Chicago, IL: American Institute of Steel Construction, p. 150.
- Behzadi-Sofiani, Behnam, Leroy Gardner, and M. Ahmer Wadee (2021). “Stability and design of fixed-ended stainless steel equal-leg angle section compression members”. In: *Engineering Structures* 249, p. 113281. DOI: [10.1016/j.engstruct.2021.113281](https://doi.org/10.1016/j.engstruct.2021.113281).
- Dassault Systems (2015a). *Abaqus 2016 Documentation*. URL: <http://130.149.89.49:2080/v2016/index.html> (visited on 11/06/2019).
- Dassault Systems (2015b). *Abaqus/CAE v.6.16*. Johnston, RI: Dassault Systems.
- de Menezes, Arthur A., Pedro C. G. da S. Vellasco, Luciano R. O. de Lima, and André T. da Silva (2019). “Experimental and numerical investigation of austenitic stainless steel hot-rolled angles under compression”. In: *Journal of Constructional Steel Research* 152, pp. 42–56. DOI: [10.1016/j.jcsr.2018.05.033](https://doi.org/10.1016/j.jcsr.2018.05.033).
- Dinis, Pedro B., Dinar Camotim, Kostas Belivanis, Colter Roskos, and Todd A. Helwig (2015). “On the buckling, post-buckling and strength behavior of thin-walled unequal-leg angle columns”. In: *Proceedings of the 2015 SSRC Annual Stability Conference*. Nashville, TN: SSRC.
- Dobrić, Jelena, Aljoša Filipović, Zlatko Marković, and Nancy R. Baddoo (2020). “Structural response to axial testing of cold-formed stainless steel angle columns”. In: *Thin-Walled Structures* 156, p. 106986. DOI: [10.1016/j.tws.2020.106986](https://doi.org/10.1016/j.tws.2020.106986).
- Dundu, Morgan (2018). “Evolution of stress–strain models of stainless steel in structural engineering applications”. In: *Construction and Building Materials* 165, pp. 413–423. DOI: [10.1016/j.conbuildmat.2018.01.008](https://doi.org/10.1016/j.conbuildmat.2018.01.008).
- Filipović, Aljoša, Jelena Dobrić, Nancy R. Baddoo, and Primož Može (2021). “Experimental response of hot-rolled stainless steel angle columns”. In: *Thin-Walled Structures* 163, p. 107659. DOI: [10.1016/j.tws.2021.107659](https://doi.org/10.1016/j.tws.2021.107659).
- Filipović, Aljoša, Jelena Dobrić, Dragan Buđevac, Nenad Fric, and Nancy R. Baddoo (2021). “Experimental study of laser-welded stainless steel angle columns”. In: *Thin-Walled Structures* 164. DOI: [10.1016/j.tws.2021.107777](https://doi.org/10.1016/j.tws.2021.107777).
- Galambos, Theodore V. (1991). “Design of axially loaded compressed angles”. In: *Proceedings of the 1991 SSRC Annual Stability Conference: "Inelastic Behavior and Design of Frames"*. Chicago, IL: SSRC, pp. 353–367.

- Gardner, L and DA Nethercot (2004). “Experiments on stainless steel hollow sections—Part 1: Material and cross-sectional behaviour”. In: *Journal of Constructional Steel Research* 60.9, pp. 1291–1318.
- Gardner, Leroy and Mahmud Ashraf (2006). “Structural design for non-linear metallic materials”. In: *Engineering structures* 28.6, pp. 926–934.
- Hill, H.N. (1944). *Determination of stress-strain relations from te offset yield strength values*. Tech. rep. Technical Note No. 927. Washington DC: National Advisory Committee for Aeronautics.
- Houska, Catherine (2014). *Designing Stainless Steel Part 1*. Conference Presentation. NASSC: The Steel Conference. Toronto, Canada.
- Hradil, Petr, Asko Talja, Esther Real, Enrique Mirambell, and Barbara Rossi (2013). “Generalized multistage mechanical model for nonlinear metallic materials”. In: *Thin-walled structures* 63, pp. 63–69.
- Kuwamura, Hitoshi (2003). “Local buckling of thin walled stainless steel members”. In: *Steel Structures* 3, pp. 191–201.
- Laracuate, Max E. (2022). “Behavior of Concentrically Loaded Austenitic Stainless Steel Single Unequal-Leg Angles”. MA thesis. University of Wisconsin - Madison.
- Laracuate, Max E., Edward J. Sippel, and Hannah B. Blum (2022). “Stability considerations of unequal-leg angle stainless steel columns”. In: *Proceedings of the 2022 SSRC Annual Stability Conference*. Denver, CO: SSRC, pp. 1–20.
- Liang, Yating, Vijaya Vengadesh Kumar Jeyapragasam, Lulu Zhang, and Ou Zhao (2019). “Flexural-torsional buckling behaviour of fixed-ended hot-rolled austenitic stainless steel equal-leg angle section columns”. In: *Journal of Constructional Steel Research* 154, pp. 43–54. DOI: 10 . 1016/j.jcsr.2018.11.019.
- Liao, KY (1982). “Compression tests of unequal-leg angles”. MA thesis. Ohio State University.
- Liu, Yi and Sabine Chantel (2011). “Experimental study of steel single unequal-leg angles under eccentric compression”. In: *Journal of Constructional Steel Research* 67.6, pp. 919–928. DOI: 10.1016/j.jcsr.2011.02.005.
- MacDonald M.; Rhodes, J.; and G. T. Taylor (2000). “Mechanical Properties of Stainless Steel Lipped Channels”. In: *CCFSS Proceedings of International Specialty Conference on Cold-Formed Steel Structures (1971 - 2018)*. Vol. 4. St. Louis, MO. URL: <https://scholarsmine.mst.edu/isccss/15iccfss/15iccfss-session11/4>.
- Meza, Francisco J., Nancy Baddoo, and Leroy Gardner (2021). “Development of Flexural Buckling Rules for the New AISC Stainless Steel Design Specification”. In: *ce/papers* 4, pp. 1537–1542. DOI: <https://doi.org/10.1002/cepa.1453>.
- Mirambell, E and E Real (2000). “On the calculation of deflections in structural stainless steel beams: an experimental and numerical investigation”. In: *Journal of Constructional Steel Research* 54.1, pp. 109–133.
- Ojalvo, Morris (2011). “Opposing Theories and the Buckling Strength of Unequal-Leg Angle Columns”. In: *Journal of Structural Engineering* 137.10, pp. 1104–1106. DOI: 10 . 1061 / (ASCE) ST.1943-541X.0000389.
- Olsson, Anders (2001). “Stainless steel plasticity : material modelling and structural applications”. PhD thesis. Luleå University of Technology, p. 298.
- Quach, WM, J Gand Teng, and Kwok Fai Chung (2008). “Three-stage full-range stress-strain model for stainless steels”. In: *Journal of Structural Engineering* 134.9, pp. 1518–1527.

- Rasmussen, Kim J. (2005). “Design of Angle Columns with Locally Unstable Legs”. In: *Journal of Structural Engineering* 131.10, pp. 1553–1560. DOI: 10.1061/(ASCE)0733-9445(2005)131:10(1553).
- Rasmussen, Kim JR (2003). “Full-range stress–strain curves for stainless steel alloys”. In: *Journal of constructional steel research* 59.1, pp. 47–61.
- Reynolds, Nicholas A. (2013). “Behavior and Design of Concentrically Loaded Duplex Stainless Steel Single Equal-Leg Angle Struts”. PhD Dissertation. Georgia Institute of Technology.
- Sarquis, Fernando R., Luciano R. O. de Lima, Pedro C. G. da S. Vellasco, and Monique C. Rodrigues (2020). “Experimental and numerical investigation of hot-rolled stainless steel equal leg angles under compression”. In: *Thin-Walled Structures* 151, p. 106742. DOI: 10.1016/j.tws.2020.106742.
- Schafer, Benjamin W., Zhanjie Li, and Cristopher D. Moen (2010). “Computational modeling of cold-formed steel”. In: *Thin-Walled Structures* 48.10-11, pp. 752–762. DOI: 10.1016/j.tws.2010.04.008.
- Sippel, Edward J. (2022). “Structural Analysis with Non-Symmetric Cross Sections”. PhD thesis. University of Wisconsin - Madison.
- Sirqueira, A. da S., P. C.G.da S. Vellasco, Luciano R. O. de Lima, and Fernando R. Sarquis (2020). “Experimental assessment of stainless steel hot-rolled equal legs angles in compression”. In: *Journal of Constructional Steel Research* 169, p. 106069. DOI: 10.1016/j.jcsr.2020.106069.
- Sun, Yao, Zhanke Liu, Yating Liang, and Ou Zhao (2019). “Experimental and numerical investigations of hot-rolled austenitic stainless steel equal-leg angle sections”. In: *Thin-Walled Structures* 144, p. 106225. DOI: 10.1016/j.tws.2019.106225.
- Timoshenko, S. and J.M. Gere (1961). *Theory of Elastic Stability*. 2nd ed. McGraw-Hill Book Company Inc., p. 177.
- Wu, Fu-hsiang (1982). “Experimental Determination of Buckling Loads for Unequal Leg Angles with Concentric Loads”. MA thesis. Ohio State University.
- Zhang, Lulu, Yating Liang, and Ou Zhao (2020). “Experimental and numerical investigations of pin-ended hot-rolled stainless steel angle section columns failing by flexural buckling”. In: *Thin-Walled Structures* 156, p. 106977. DOI: 10.1016/j.tws.2020.106977.
- Zhang, Lulu, Yating Liang, and Ou Zhao (2021). “Laboratory testing and numerical modelling of pin-ended hot-rolled stainless steel angle section columns failing by flexural-torsional buckling”. In: *Thin-Walled Structures* 161, p. 107395. DOI: 10.1016/j.tws.2020.107395.
- Zhang, Lulu, Kang Hai Tan, and Ou Zhao (2019). “Experimental and numerical studies of fixed-ended cold-formed stainless steel equal-leg angle section columns”. In: *Engineering Structures* 184. September 2018, pp. 134–144. DOI: 10.1016/j.engstruct.2019.01.083.
- Zhang, Ying, Yidu Bu, Yuanqing Wang, Zhongxing Wang, and Yuanwen Ouyang (2021). “Study of flexural–torsional buckling behaviour of 6061-T6 aluminium alloy unequal-leg angle columns”. In: *Thin-Walled Structures* 164, p. 107821. DOI: 10.1016/j.tws.2021.107821.
- Zhang, Ying, Yuanqing Wang, Zhongxing Wang, Yidu Bu, Shenggang Fan, and Baofeng Zheng (2020). “Experimental investigation and numerical analysis of pin-ended extruded aluminium alloy unequal angle columns”. In: *Engineering Structures* 215, p. 110694. DOI: 10.1016/j.engstruct.2020.110694.
- Ziemian, Ronald D. (2010). *Guide to stability design criteria for metal structures*. 6th. John Wiley & Sons.